Reduced Nicotinamide Mononucleotide (NMNH) Potently Enhances NAD^+, Causes Reductive Stress, and Suppresses Glycolysis and Cell Growth

Yan Liu [1,2,4], Chengting Luo [1,2,4], Ting Li [2,4], Wenhao Zhang [1], Zhaoyun Zong [2], Xiaohui Liu [2,3*], Haiteng Deng [2, 3, 5,*]

[1]Tsinghua University-Peking University Joint Center for Life Sciences, Tsinghua University, Beijing, 100084, China

[2]MOE Key Laboratory of Bioinformatics, Centre for Synthetic and Systems Biology, School of Life Sciences, Tsinghua University, Beijing, 100084, China

[3]National Center for Protein Science, Tsinghua University, Beijing, 100084, China

[4]These authors contributed equally

[5]Lead Contact

*Correspondence: dht@mail.tsinghua.edu.cn (Haiteng Deng)

xiaohui2013@mail.tsinghua.edu.cn (Xiaohui Liu)

ABSTRACT

In the present study, we developed a chemical method to produce dihydro nicotinamide mononucleotide (NMNH), which is the reduced-form of nicotinamide mononucleotide (NMN). We demonstrated that NMNH was a better NAD^+ enhancer compared to NMN both *in vitro* and *in vivo* mediated by NMNAT. More importantly, NMNH significantly increased the reduced NAD (NADH) levels in cells and in mouse liver, resulting in cellular reductive stress and elevated reactive oxygen species. NMNH also induced cell cycle arrest and suppressed cell growth. Metabolomic analysis revealed that NMNH inhibited glycolysis and TCA cycle. However, NMNH treatment did not cause observable difference in mice. Taken together, our work demonstrates that NMNH is a potent NAD^+ enhancer, and induces reductive stress to suppress cell growth.

KEY WORDS

Nicotinamide Adenine Dinucleotide (NAD^+ and NADH), Reduced Nicotinamide Mononucleotide (NMNH), Reductive Stress, Cell Growth, Glycolysis, TCA cycle

INTRODUCTION

Nicotinamide adenine dinucleotide (NAD^+) is essential to living organisms because it participates in hundreds of biological reactions and regulates key biological processes, such as metabolism and DNA repair (Canto et al., 2015; Magni et al., 2004). Previous studies revealed that upregulating NAD^+ biosynthesis by genetic manipulation leads to increased stress resistance and elongated lifespan in yeast and *Drosophila* (Anderson et al., 2002; Anderson et al., 2003; Balan et al., 2008). Increasing NAD^+ level is proved to delay progeroid and other degenerative disease in mice (Fang et al., 2014; Rajman et al., 2018). There is ample evidence that nicotinamide riboside (NR) and nicotinamide mononucleotide (NMN) are potent NAD^+ enhancers, as they increase cellular NAD^+ levels and confer multiple health benefits (Yoshino et al., 2018). Supplementation with NR or NMN protects mice against age-associated health deterioration (Yoshino et al., 2011; Zhang et al., 2016).

These studies mainly focused on NAD precursors in the oxidized form since most NAD^+ consuming enzymes uses NAD^+ as the substrate. Less is known about the roles of NAD precursors in the reduced form. Two recent studies revealed that NR in its reduced form, denoted as NRH, was a better NAD^+ booster than NR or NMN in cells and tissues (Giroud-Gerbetant et al., 2019; Yang et al., 2019). Sauve et al. also showed

that NRH increased resistance to cell death caused by genotoxins and the conversion of NRH to NMNH was independent of Nrk1 or Nrk2. Canto et al. found that NRH was converted to NMNH by adenosine kinase to synthesize NAD^+, and demonstrated that NRH was orally available and prevented cisplatin-induced acute kidney injury in mice. However, it has not been reported, to the best of our knowledge, whether the reduced form of NMN can increase cellular NAD^+ levels and regulate biological processes.

In the present work, we developed a chemical reduction method for synthesizing the reduced NMN, denoted as NMNH and investigated the biological effects of NMNH on cellular processes. We found that NMNH was a better NAD^+ enhancer than NMN both *in vitro* and *in vivo*. More strikingly, NMNH increased cellular NADH levels, induced reductive stress, and suppressed cell growth, glycolysis and TCA cycle.

RESULTS

NMNH increased cellular NAD^+ levels

We investigated enzymatic and chemical synthesis methods for preparing NMNH and found that NMNH generated from chemical synthesis had a high yield and high purity. The procedure for NMNH synthesis is displayed in Figure 1A. NMNH was produced by reduction of NMN using thiourea dioxide (TDO). We chose TDO as the reducing reagent based on the facts that TDO is stable in common laboratory storage conditions, and it is amenable to solution preparation. TDO possesses high reduction potential in aqueous solutions and is also suitable for scalable applications. Briefly, 340 mg NMN and 125 mg TDO were dissolved in 1 mL of 10% ammonia solution. The

reaction mix was incubated at 40℃ for 1 hour and the product was then purified by HPLC using an amide column followed by vacuum drying. Purified NMNH was in orange color and had a UV absorption centered at 340 nm (Figure S1A). The reaction product was characterized by high resolution mass spectrometry. The mass to charge ratio (m/z) of the final product was determined to be 335.0648 in negative ion mode, which matches the theoretical molecular weight of NMNH (Figure S1B) with an elemental composition of C11H17N2O8P1. These results suggest that the reduction product is NMNH.

To further verify the identity of the reaction product, we generated NMNH from NADH using NADH pyrophosphatase (NudC), which decomposes NADH into NMNH and AMP (Frick and Bessman, 1995). The NADH decomposition reaction is shown in Figure S1C. The NudC-generated product was analyzed using high resolution mass spectrometry and the major peak was observed with mass to charge ratio (m/z) 335.0633 in negative ion mode (Figure S1D), precisely matching the mass of the reduction-generated NMNH. We compared the MS/MS spectra of enzymatically- and chemically-generated NMNH and found that they shared an identical fragmentation pattern (Figure S1E). Therefore, we confirmed that reduction of NMN by TDO produces NMNH. These results show that this reduction method is robust and effective. We examined the stability of NMNH and found that NMNH was stable under alkaline pH and low temperature conditions (Figure S1F). The half-life of NMNH at pH 7.0 and at room temperature was about 2.4 days, which is much longer than the half-life of NRH, which is 3 h at pH 6.0 and at room temperature (Yang et al., 2019).

We next examined the effects of NMNH on enhancing cellular NAD^+ levels as compared to NMN. NMNH (100 μM) treatment increased the level of cellular NAD^+ by 5-7 folds in HepG2 cells whereas 100 μM NMN only slightly increased the level of NAD^+, as determined by mass spectrometry (Figure 1B and Figure S1G). These results indicate that, compared with NMN, NMNH is a more efficient NAD^+ enhancer. In addition to HepG2 cells, we also confirmed that NMNH enhanced the NAD^+ in ES-2 cells and 3T3-L1 cells, which are human ovary derived cells and mouse embryo fibroblast derived cells, respectively (Figure 1C and 1D). We found that NMNH increased cellular NAD^+ levels in time- and concentration-dependent manner in 786-O cells (Figure S1H and S1I). Sirtuins are key NAD^+-dependent deacetylases that play important roles in regulating biological functions, such as stress-resistance and DNA damage and generates NAM as one of the end products (Imai and Guarente, 2014). We found that NMNH increased cellular NAM concentration (Figure 1E), which indicated that NMNH promoted sirtuins' activity. We examined cellular lysine-acetylation and found that both NMN and NMNH promoted cellular deacetylation activity with NMNH being more efficient than NMN (Figure S1J). We further examined the effects of NMNH on NAD^+ levels using a mouse model. We treated C57BL/6J male mice with 340 mg/kg NMN or NMNH via intraperitoneal injection and measured liver NAD^+ concentrations by mass spectrometry. We found that the liver NAD^+ level was 4-fold higher in NMNH-treated mice than that in PBS-treated mice (Figure 1F). Additionally, the liver NAD^+ level in NMNH-treated mice was 1.5-fold higher than that in NMN-treated mice. These results demonstrate that NMNH is a more potent *in vivo*

NAD^+ enhancer than NMN. NMNH also significantly increased levels of NAM in mouse liver (Figure 1G).

NMNH Induced Reductive Stress and Repressed Cell Growth

It has been proposed that NRH is converted to NMNH, which is further converted to NADH by NMNAT (Berger et al., 2005; Giroud-Gerbetant et al., 2019). To examine whether NMNH increases the cellular NADH concentration, we measured NADH using mass spectrometry. We found that NADH levels were 2.5-fold higher in NMNH-treated HepG2 cells than in untreated and NMN-treated cells (Figure 2A). Increased NADH level was also detected in NMNH-treated 786-O cells (Figure S2A). We uncovered that NMNH treatment increased NADH level by 3 folds in mouse liver (Figure S2B). Excessive NADH has been shown to generate reductive stress, resulting in increased cellular oxygen radicals and hydrogen peroxide (Kussmaul and Hirst, 2006; Xiao and Loscalzo, 2019). To explore whether NMNH promotes reductive stress, we treated HepG2 cells with NMNH and measured cellular ROS using CellROX® Deep Red Reagents (Invitrogen, NY). We found that NMNH increased cellular ROS levels by 1.4 folds in 24 h in HepG2 cells as compared to the untreated cells (Figure 2B).

It is known that high level ROS inhibit cell growth (Verbon et al., 2012). We explored the effect of NMNH on cell growth and found that NMNH treatment inhibited HepG2 cell growth at concentrations higher than 250 μM (Figure 2C). We performed data dependent quantitative proteomic analysis to identify differentially expressed proteins (DEPs) of HepG2 under 1 mM NMNH treatment for 12 h. 6142 proteins were

identified using biological triplicates with false-positive rate less than 1%. The fold change cutoff was determined according to 88% coverage of percentage variations (Figure S2C) and proteins with the fold change more than 1.3 or less than 0.77 were considered as DEPs[31, 32]. Based on tandem mass tag (TMT) ratio in proteins with 2 or more unique peptides, we identified 289 up-regulated proteins and 171 down-regulated proteins (Figure S2D). Ingenuity Pathway Analysis (IPA) revealed that NMNH treatment affected cell cycle progression (Figure S2E). We analyzed the cell cycle in HepG2 cells treated with 1 mM NMNH or NMN for 12 h, respectively and uncovered that NMNH caused cell cycle arrest whereas NMN had no effects on cell cycles (Figure 2D). To further examine the effects of NMNH on cell growth, we treated 786-O cells with different concentrations of NMNH. 786-O cells, derived from a clear cell renal cell carcinoma (ccRCC) patients, exhibits a typical Warburg phenotype and their growth were dependent on glycolysis (Tang et al., 2016; Teng et al., 2019). We measured the growth curve of 786-O cells and found that 500 μM NMNH completely blocked cell growth (Figure 2E). Further analysis revealed that NMNH inhibited cell growth in 786-O cells at 50 μM (Figure 2F), whereas 250 μM NMNH was needed to effectively inhibit cell growth in HK-2 cells (Figure 2F), which was an immortalized proximal tubule epithelial cell line from normal adult human kidney (Ryan et al., 1994). To verify whether NMNH shows any repression effect in animal, we treated C57BL/6J male mice with 13.6 mg/kg NMN or NMNH via intraperitoneal injection every day for 4 weeks and found no difference in body weight curves among PBS-treated, NMNH- and NMN-treated mice, as shown in Figure S2F.

NMNH inhibited Glycolysis and TCA Cycle

Previous studies indicated that accumulation of NADH slowed down glycolysis and TCA cycle (Kosicki and Lee, 1966; Tilton et al., 1991). To examine cellular metabolic responses to NMNH treatment, we carried out metabolomic profiling on NMNH- and NMN-treated cells. We found that NMNH treatment decreased levels of glycolysis intermediates, including fructose-1,6-diphosphate, DHAP, 3PG / 2PG, PEP and pyruvate (Figure S3A). NMNH treatment also decreased the levels of TCA cycle intermediates, including citrate, cis-aconitate, isocitrate, succinate, and malate (Figure S3B). These results indicated that NMNH-generated NADH accumulation inhibits cellular glycolysis and the TCA cycle.

We further carried out isotope tracing experiment using $^{13}C_6$-glucose to trace the regulation of glycolysis and TCA cycle by NMNH. As shown in Figure 3A, intermediates including glucose-6-phosphate (M+6), 3-phosphoglycerate (3PG) / 2-phosphoglycerate (2PG) (M+3), phosphoenolpyruvate (PEP) (M+3) and pyruvate (M+3) declared significantly reduced glycolysis pathway by NMNH treatment. The results demonstrated that NMNH repressed cellular glycolysis. Meanwhile, the production of TCA cycle intermediates from glycolysis was clearly suppressed by NMNH based on the results of citrate (M+2), α-ketoglutarate (M+2), succinate (M+2) and malate (M+2) in Figure 3B. However, NMN treatment revealed distinct regulation of glycolysis and TCA cycle. NMN only induced mild decrease of 2PG/3PG and PEP in glycolysis (Figure 3A) and almost no observable reduction of TCA cycle in cells

(Figure 3B). These results suggested that NMNH has very significant suppression of glycolysis and TCA cycle while NMN also hindered the glycolysis but with much milder extent.

NMNAT catalyzed NAD^+ biosynthesis from NMNH

Our results demonstrated that the cellular NAD^+ and NADH levels were elevated dramatically by NMNH. In order to investigate the specific mechanism of NMNH to enhance the biosynthesis NAD^+ and NADH, the isotope tracing was performed using $^{13}C_6$-glucose. The tracer of $^{13}C_6$-glucose enables to provide the ribosyl labeling either through NMN from PRPP or ATP from purine biosynthesis (Figure S4). Four different labeling status were monitored using TSQ mass spectrometer as shown in Figure 4A. Interestingly, unlike TCA cycle regulation, NMN and NMNH treatments illustrated similar trend of NAD^+ and NADH biosynthesis reprogramming (Figure 4B and 4C). The incorporation of exogenous NMN or NMNH stimulated the biosynthesis of NAD^+ and NADH, which resulted in the enhanced labeling from ATP (M+5-A). However, NMNH had more striking effect to stimulate NAD^+ and NADH biosynthesis with almost completely inhibiting endogenous NMN synthesis by NAMPT. We detected NMNH in NMNH-treated cells but not in NMN-treated cells or untreated cells, indicating that NMNH was able to enter cells (Figure S4B). The recent study suggested that NRH was phosphorylated to NMNH which was further converted to NADH by NMNAT for boosting cellular NAD^+ content (Giroud-Gerbetant et al., 2019). Tannic acid, which is a specific NMNAT inhibitor (Giroud-Gerbetant et al., 2019), was used to explore the

contribution of NMNAT in NAD+ biosynthesis (Figure S4C). Meanwhile, the effect of FK866 was also examined as a potent NAMPT inhibitor. The results suggested that tannic acid almost abolished the NAD^+ increasing effect of NMNH while FK866 only showed slightly inhibitory effect (Figure S4C).

It was also found that the cellular NMN level was increased by NMNH even more dramatically than NMN treatment. (Figure S4D). Besides, the isotope tracing results showed < 0.4% of ribosyl labeled NMN in NMNH treated cells (Figure S4E), which suggested that the increased NMN was not biosynthesized from NAM and PRPP. This gave the hint of NMN production from NMNH in cells. Former reports indicated that ribosyldihydronicotinamide dehydrogenase (NQO2) could use NRH or a variety of its analogues as electron donors to reduce quinones to generate NR or relative dehydrogenation products (Fu et al., 2008; Wu et al., 1997). It provided the possibility that NQO2 may have the function of turning NMNH to NMN. Herein, the potent NQO2 inhibitor quercetin was used to investigate the role of NQO2 in NAD^+ biosynthesis (Wu et al., 1997). The repression of the NAD^+ increasing effect by NMNH was observed (Figure S4C), suggesting NQO2 played a role in NMNH-induced NAD^+ synthesis. Based on the results, we suggested that NMNH increased cellular NAD^+ content in two ways that NMNH was directly converted to NADH or it was firstly converted to NMN and then to NAD^+, as shown in Figure 4D.

DISCUSSION

NAD^+ is an important regulator of health and longevity (Houtkooper et al., 2012;

Imai et al., 2000). Dozens of human clinical trials of NAD^+ precursors are ongoing or recruiting participants currently while the existing data suggest that the translation from mouse model to human is not straightforward as people thought (Katsyuba et al., 2020). Therefore, finding new agents that boost NAD^+ levels is important to increase candidates for improving human health, especially for elderly people. Herein, we established a reduction method for efficient preparation of NMNH from NMN. Our study supports previous findings that the reduced form of NAD^+ precursors (NMNH and NRH) are better NAD^+ enhancers than their corresponding ones in oxidized form both *in vitro* and *in vivo*. Meanwhile, we confirmed that long-term administration of NMNH is safe. Unlike previous studies showing that NRH had little effect on cell growth (Giroud-Gerbetant et al., 2019; Yang et al., 2019), we found that NMNH treatment caused cell cycle arrest and inhibited cell growth even at a concentration of 100 μM.

Sauve *et al* reported that NRH substantially increased NAD^+ / NADH ratio in cultured cells and in liver suggesting that NRH only mildly increased NADH levels. However, NMNH significantly increased cellular NADH levels, especially in liver. NAD^+ and NADH are an essential cellular redox couple and are inter-converted (Ying, 2008). NADH is the electron carrier in respiratory chain for ATP generation (Weiss et al., 1991). Increased cellular NADH concentration has been reported to induce reductive stress to increase reactive oxygen species (ROS) and a recent study showed that reductive stress can inhibit tumor growth (Gao et al., 2019; Xiao and Loscalzo, 2019). We suggest that NMNH-induced reductive stress, which increased cellular ROS, contributes to cell growth inhibition. We identified that NMNH suppressed glycolysis as

well as the TCA cycle by metabolomics and isotope tracing analysis, which also represses cell growth.

We also deconstructed NAD^+ synthesis pathway induced by NMNH. We found that NMNH enter cell to increased NAD^+ content through NMNAT but not NAMPT. Moreover, we suggest that NMNH treatment inhibited NAD^+ synthesis through NAMPT for little NAD^+ (M+5-N) and NAD^+ (M+10) were detected, while NMN treatment showed less effect. We further suggested that NMNH were converted to NMN to synthesize NAD^+. We demonstrated that NQO2 was a candidate to catalyze the conversion from NMNH to NMN but there may be other proteins able to catalyze this process.

In summary, we developed a chemical reduction method to produce NMNH in high yield. Our results demonstrate that NMNH is a potent NAD^+ enhancer *in vitro* and *in vivo*. NMNH also significantly increased cellular NADH levels, which induced reductive stress, repressed glycometabolism and inhibited cell growth.

SIGNIFICANCE

NAD^+ is an essential metabolite in living organisms and has been reported to be a health-promotion molecule. Here, we introduce a method to generate the reduced-form NAD^+ precursor, NMNH, which is a potent NAD^+ enhancer both *in vitro* and *in vivo*. Besides, we found that NMNH can repress cell growth, induce reductive stress and suppress glycolysis and TCA cycle. Contrast to NMN, which is the direct precursor of NAD^+, NMNH is the direct precursor of NADH. Using proteomics and metabolomics technologies, our work demonstrated the effects of NMNH, which is a reduced-form

NAD^+ precursor, on cell metabolism. The significance of our findings is that we demonstrated a new potent NAD^+ enhancer and explored the biological effects of NAD^+ precursor in reduced form.

ACKNOWLEGEMENT

We thank the Protein Chemistry Facility at Protein Research Technology Center of Tsinghua University for sample analysis. We thank the Metabolomics Facility at Technology Center for Protein Sciences of Tsinghua University for sample analysis. We thank the Cell Biological Facility at the Center for Biomedical Analysis of Tsinghua University for FACS analysis. We thank Michelle Goody, PhD, from Liwen Bianji, Edanz Editing China (www.liwenbianji.cn/ac), for editing the English text of a draft of this manuscript. This study was supported by the Chinese Ministry of Science and Technology (grant No. 2017ZX10201101 and No. 2014CBA02005), China Postdoctoral Science Foundation (grant No. 2017M610080), National Key Research and Development Program (grant No. 2017YFA0505103), National Nature Science Foundation of China (grant No. 21877068), and Shandong Science and Technology Committee.

AUTHOR CONTRIBUTIONS

Conceptualization, Y.L. and H.D.; Methodology, Y.L., C.L., T.L., W.Z., Z.Z., X.L. and H.D.; Investigation, Y.L., C.L. and T.L.; Validation, Y.L., C.L. and T.L.; Writing – Original Draft, Y.L. and T.L.; Writing – Review & Editing, Y.L., X.L. and H.D.; Funding Acquisition, H.D.; Supervision, H.D.

DECLARATION OF INTERESTS

The authors declare no conflicts of interest.

Methods

NMNH preparation

NMNH was prepared by reducing NMN with TDO. Briefly, 340 mg NMN and 125 mg TDO were mixed in 1 mL 10% ammonia solution and incubated in 40℃ water bath for 1 h. Next, NMNH was purified by a Dionex UltiMate 3000 (Thermo Scientific) HPLC system with an amide column (Waters, XBridge, 10 × 250 mm). Mobile phase A was prepared by adjusting HPLC-grade water to pH 10.0 using ammonia solution and mobile phase B was prepared by adjusting HPLC-grade acetonitrile to pH 10.0 using ammonia solution. Follow rate was set at 3 mL / min and the gradient was as follows: 0 min, 90% B; 5min, 90% B; 45 min, 40% B; 50 min, 40% B; 55 min, 90% B; 60 min, 90% B. The fraction with 340 nm absorption was collected and concentrated by vacuumdrying. NMNH was also generated by enzymatic decomposing NADH using NudC. Briefly, 20 mg NADH and 13 μg NudC were dissolved in 1 mL H_2O containing 500 mM ammonium acetate and 3 mM magnesium chloride. The mixture was incubated in 48℃ water bath for 1 h. Characteristic absorption feature and stability of NMNH were characterized using the same HPLC system, mobile phases and follow rate. The gradient was as follows: 0 min, 90% B; 5 min, 90% B; 15 min, 40% B; 18 min, 40% B; 19 min, 90% B; 20 min; 90% B.

NudC expression and purification

DNA corresponding to the NudC open reading frame was synthesized (QINGLAN BIOTECH) and integrated into pET21b vector. Expression plasmid was transformed into C41 (DE3) competent cell (TianWeiTaiDa, China). Briefly, *E. coli* cells transformed with expressing plasmid were cultured in LB media until OD_{600} reached 0.6 and protein expression was induced by 1mM IPTG. Harvested cells were lysed by ultrasonication in lysis buffer (300 mM NaCl, 50 mM NaH2PO4, 10 mM imidazole, pH 8.0). Cell lysates were centrifuged at 15, 000×*g* for 30 min and the supernatants were purified by Ni-NTA agarose (Qiagen) and desalted using a HiTrap Desalting column (GE Healthcare).

Mass spectrometric analysis of NMNH

NMNH products were analyzed by a Q Exactive mass spectrometer (Thermo Scientific™) connected to a Dionex UltiMate 3000 (Thermo Scientific) HPLC system without column in negative ion mode. The mobile phase A was prepared by adjusting HPLC-grade water to pH 10.0 using ammonia solution. Follow rate was set at 0.2 mL / min and gradient was as follows: 0 min, 100% A; 5min, 100% A. Detailed mass spectrometer parameters were set as follows: spray voltage was set at 3.5 kV; capillary temperature was set at 250℃; sheath gas flow rate (arb) was set at 45; aux gas flow rate (arb) was set at 10; mass range (m/z) was set at 80-750; full MS resolution was set at 70, 000; MS/MS resolution was set at 17, 500; topN was set at 10; HCD energy was set at 20, 30, 40.

Cell lines

Human hepatocellular carcinoma cell line HepG2 (male), human renal cell adenocarcinoma cell line 786-O (male), human ovary clear cell carcinoma cell line ES-2, mouse embryo fibroblast cell line 3T3-L1 and human kidney cell line HK-2 (male) were purchased from the cell bank of Chinese Academy of Sciences (Shanghai, China). HepG2 and 786-O cells were cultured in RPMI1640 medium (Wisent, Canada) with 10% fetal bovine serum (PAN-Biotech, Germany) and 1% penicillin and streptomycin (Wisent, Canada) supplementation. ES-2 cells were culture in McCoy's 5A medium (Gibco) with 10% fetal bovine serum (PAN-Biotech, Germany) and 1% penicillin and streptomycin (Wisent, Canada) supplementation. 3T3-L1 cells were cultured in DMEM (Wisent, Canada) medium with 10% fetal bovine serum (PAN-Biotech, Germany) and 1% penicillin and streptomycin (Wisent, Canada) supplementation. HK-2 cells were cultured in Defined Keratinocyte SFM (Gibco) supplemented with 2.5 μg / 500 mL EGF recombinant human protein (Gibco) and 1% penicillin and streptomycin (Wisent, Canada). Cells were cultured in cell incubator containing 5% CO_2 at 37 ℃.

In vivo experiments

Wild type C57BL/6J male mice, weighing 25±3g, 8 weeks old were used for experiment, which were randomly divided into three groups including PBS-treated group, NMNH treated group and NMN treated group. All the mice were housed in a temperature and light regulated room in a SPF facility and received food or water *ad libitum*. All animal experiments conform to the guidelines of the Laboratory Animal Research Center of Tsinghua University. All animal protocols used in this study were approved by the Institutional Animal Care and Use Committee of Tsinghua University.

Metabolomic analysis

Polar metabolites were extracted from cells and tissues (mouse liver) using pre-chilled 80% methanol (vol / vol). For cell samples, cells were washed for three times using cold PBS to avoid serum contamination and stored at -80 ℃ for 2 h after addition of 2 mL of 80% methanol. Cells were transferred into 1.5 mL tubes and the supernatants were harvested after centrifugation. The supernatants were dried by vacuum drying and stored -80 ℃ before analyzing. The pellets were dissolved using 1 M KOH for protein concentration determination. Metabolite samples were redissolved using 80% methanol according to protein concentration for mass spectroscopy analysis. For tissue samples, 25 mg tissues were homogenized in 250 μL pre-chilled 80% methanol and stored at -80 ℃ for 2 h. Samples were centrifuged and supernatants of the same volume were transferred into new 1.5 mL tubes. The supernatants were dried by vacuum drying and redissolved using the same volume of 80% methanol for mass spectroscopy analysis.

Polar metabolites were analyzed by a Q Exactive Orbitrap mass spectrometer (Thermo, CA) or a TSQ Quantiva Ultra triple-quadrupole mass spectrometer (Thermo Fisher, CA). For Q Exactive Orbitrap mass spectrometer analysis, an Ultimate 3000 UHPLC (Dionex) was coupled to the mass spectrometer which was in positive mode. Atlantis HILIC Silica column (2.1×100 mm, Waters) was used for sample separation. In positive mode, mobile phase A was prepared by dissolving 0.63 g of ammonium formate in 50 ml of HPLC-grade water followed by adding 950 ml of HPLC-grade

acetonitrile and 1 μl of formic acid. Mobile phase B was prepared by dissolving 0.63 g of ammonium formate in 500 ml of HPLC-grade water followed by adding 500 ml of HPLC-grade acetonitrile and 1 μl formic acid. The elution gradient was as follows: 0 min, 1% B; 2 min, 1% B; 3.5 min, 20% B; 17 min, 80% B; 17.5 min, 99% B; 19 min, 99% B; 19.1 min, 1% B; 22 min, 1% B. In negative mode, mobile phase A was prepared by 0.77 g of ammonium acetate in 50 ml of HPLC-grade water followed by adding 950 ml of HPLC-grade acetonitrile and pH was adjusted to 9.0 using ammonium hydroxide. Mobile phase B was prepared by dissolving 0.77 g of ammonium acetate in 500 ml of HPLC-grade water followed by adding 500 ml of HPLC-grade acetonitrile and pH was adjusted to 9.0 using ammonium hydroxide. The elution gradient was as the same as positive mode. Detailed parameters of mass spectrometer were as follows: spray voltage was set at 3.5 kV; capillary temperature was set at 275°C; sheath gas flow rate (arb) was set at 35; aux gas flow rate (arb) was set at 8; mass range (m/z) was set at 70–1050; full MS resolution was set at 70,000; MS/MS resolution was set at 17,500; topN was set at 10; NCE was set at 15/30/45; duty cycle was set at 1.2 s.

For TSQ Quantiva Ultra triple-quadrupole mass spectrometer analysis, a Dionex Ultimate 3000 UPLC system was coupled to the mass spectrometer, equipped with a heated electrospray ionization (HESI) probe. Extracts were separated by a synergi Hydro-RP column (2.0×100mm, 2.5 μm, phenomenex). A binary solvent system was used, in which mobile phase A consisted of 10 mM tributylamine adjusted with 15 mM acetic acid in water, and mobile phase B of methanol. This analysis used a 25-minute gradient from 5% to 90% mobile B. Positive-negative ion switching mode was performed for data acquisition. Cycle time was set as 1 s. The resolutions for Q1 and Q3 are both 0.7 FWHM. The source voltage was 3.5 kV for positive and 2.5 kV for negative ion mode. The source parameters are as follows: spray voltage was set at 3.0 kV; capillary temperature was set at 320°C; heater temperature was set at 300°C; sheath gas flow rate was set at 35; auxiliary gas flow rate was set at 10. Data analysis and quantitation were performed by the software Tracefinder 3.1.

Western blot assay

Cells were harvested and lysed using RIPA lysis buffer (Beyotime, China) supplemented with 1% protease inhibitor cocktail (MERCK, Germany). After centrifugation at 14, 000×*g* for 15 min at 4°C, supernatants were collected and protein concentrations were determined using BCA protein assay kit (Solarbio, Beijing, China). Proteins of equal amounts were separated using 12% SDS-PAGE gel and transferred onto PVDF membrane. Western blot assay followed a standard procedure. Anti-acetyl-lysine antibody was purchased from MILLIPORE (4G12), anti-actin antibody was purchased from Cell Signaling Technology (13E5), anti-rabbit antibody was purchased form Cell Signaling Technology (7074S) and anti-mouse antibody was purchased from Cell Signaling Technology (7076S).

Cellular total NAD^+ concentration or NADH concentration measurement by kit

Intracellular total NAD^+ concentration or NADH content was measured using NAD^+ / NADH detecting kit (Beyotime, China) following manufacture's instruction. Briefly, cell media were removed and cells were washed with PBS. Cold NAD^+ / NADH extraction buffer was added to cells for cell lysis. Then the lysis was centrifuged (12, 000×*g*, 10 min, 4 ℃).For cellular total NAD^+ concentration measurement, cell lysis supernatants and NADH standards were added into 96-well plate and mixed with ethanol dehydrogenase working solution and incubated at 37 ℃ for 10 min. Color reagent was then added to the mix and the absorbance at 450 nm was measured. For cellular NADH concentration measurement, cell lysis supernatants and NADH standards were heated at 60 ℃ for 1 h and were then added into 96-well plate and mixed with ethanol dehydrogenase working solution and incubated at 37 ℃ for 10 min. Color reagent was then added to the mix and the absorbance at 450 nm was measured. Total NAD^+ concentration or NADH concentration was calculated according to standard curve. The concentration measurements were detected in triplicate and data were analyzed using Student's t-test.

Cellular reactive oxygen species detection

Cellular reactive oxygen species (ROS) were detected using CellROX® Deep Red Reagents (Invitrogen, NY) following the manufacturer's instruction. Briefly, cells in 6-well plates were harvested and washed with PBS and incubated in media containing 1 μM CellROX Deep Red reagent at 37 ℃ for 1 h. Cells were then analyzed on a BD FACS Aria Ⅱ Flow Cytometer (Becton Dickinson, NJ). Cellular ROS levels were detected in triplicate and data were analyzed using Student's t-test.

Cell proliferation assay

Cells were seeded in 96-well plates at proper density and cultured according to experimental requirement. Cell proliferation rates were determined with a Cell Counting Kit-8 (CCK-8) (Dojindo Laboratories, Kumamoto, Japan). Briefly, media were removed and cells were washed with PBS and incubated with media containing 10% CCK-8 (vol / vol) at 37 ℃ for 2 h. 450 nm absorbance was measured to represent relative cell number. Cell proliferation assays were performed in triplicate and data were analyzed using Student's t-test.

Proteomic analysis

200 μg proteins were extracted using 8 M urea followed by reduction and alkylation. Then, proteins were digested with trypsin (Promega, Fitchburg, WI) for 14 hours at 37 ℃. Peptides were then desalted and labeled by tandem mass tag (TMTsixplex™, Thermo) according to manufacturer's protocol. Next, samples were mixed, desalted and separated by HPLC and analyzed by Orbitrap Fusion™ Lumos™ Tribrid™ mass spectrometer (Thermo Scientific™). The MS/MS spectra were searched against the Uniprot human database (release date of October, 06, 2019, 20352 sequences) using the SEQUEST searching engine of Proteome Discoverer 2.1 software. The experiments were performed with three biological repeats.

Cell cycle determination

HepG2 cells were harvested after 1 mM NMNH or NMN treatment for 12 h and washed with PBS containing 1% FBS. PBS were removed and cells were resuspended using 70% pre-chilled ethanol. Cells were fixed over night in 4 ℃. Ethanol were then removed and cells were resuspended using PBS supplemented with 40 μg / mL propidium iodide (PI, Leagene, China) and RNase (TIANGEN, China). Cell cycle analysis was performed on a BD Calibur Cytometer (Becton Dickinson, NJ)

Isotope tracing metabolomic analysis

RPMI1640 medium that was glucose-free (Gibco, Thermo Fisher Scientific, USA) was supplemented with 11 mM $^{13}C_6$-glucose (Cambridge Isotope Laboratories, USA) for cell culture. HepG2 cells were culture in $^{13}C_6$-glucose RPMI1640 media supplemented with 1 mM NMNH or NMN for 6 h before metabolomic analysis. An unlabeled culture was prepared for unlabeled metabolites identification by adding equal concentration of unlabeled glucose instead of $^{13}C_6$-glucose. Sample preparation and analyzing method was described in “Metabolomic analysis” section. Isotope tracing metabolomic analysis was performed using a TSQ Quantiva Ultra triple-quadrupole mass spectrometer.

Statistical method

GraphPad Prism 7.00 was used for statistical analysis. Data were shown as mean ± SEM and Student’s t test was employed to determine significant differences (*$p < 0.05$, **$p < 0.01$, ***$p < 0.001$, ****$p < 0.0001$). p values of < 0.05 were considered to be significant. Significance is obtained compared to the untreated group unless otherwise specified.

Reference

Anderson, R.M., Bitterman, K.J., Wood, J.G., Medvedik, O., Cohen, H., Lin, S.S., Manchester, J.K., Gordon, J.I., and Sinclair, D.A. (2002). Manipulation of a nuclear NAD(+) salvage pathway delays aging without altering steady-state NAD(+) levels. J

Biol Chem *277*, 18881-18890.

Anderson, R.M., Bitterman, K.J., Wood, J.G., Medvedik, O., and Sinclair, D.A. (2003). Nicotinamide and PNC1 govern lifespan extension by calorie restriction in Saccharomyces cerevisiae. Nature *423*, 181-185.

Balan, V., Miller, G.S., Kaplun, L., Balan, K., Chong, Z.Z., Li, F.Q., Kaplun, A., VanBerkum, M.F.A., Arking, R., Freeman, D.C.*, et al.* (2008). Life span extension and neuronal cell protection by Drosophila nicotinamidase. J Biol Chem *283*, 27810-27819.

Berger, F., Lau, C., Dahlmann, M., and Ziegler, M. (2005). Subcellular compartmentation and differential catalytic properties of the three human nicotinamide mononucleotide adenylyltransferase isoforms. J Biol Chem *280*, 36334-36341.

Canto, C., Menzies, K.J., and Auwerx, J. (2015). NAD(+) Metabolism and the Control of Energy Homeostasis: A Balancing Act between Mitochondria and the Nucleus. Cell Metab *22*, 31-53.

Fang, E.F., Scheibye-Knudsen, M., Brace, L.E., Kassahun, H., SenGupta, T., Nilsen, H., Mitchell, J.R., Croteau, D.L., and Bohr, V.A. (2014). Defective Mitophagy in XPA via PARP-1 Hyperactivation and NAD(+)/SIRT1 Reduction. Cell *157*, 882-896.

Frick, D.N., and Bessman, M.J. (1995). Cloning, Purification, and Properties of a Novel Nadh Pyrophosphatase - Evidence for a Nucleotide Pyrophosphatase Catalytic Domain in Mutt-Like Enzymes. J Biol Chem *270*, 1529-1534.

Fu, Y., Buryanovskyy, L., and Zhang, Z. (2008). Quinone reductase 2 is a catechol quinone reductase. J Biol Chem *283*, 23829-23835.

Gao, X., Wei, K., Hu, B., Xu, K., and Tang, B. (2019). Ascorbic acid induced HepG2 cells' apoptosis via intracellular reductive stress. Theranostics *9*, 4233-4240.

Giroud-Gerbetant, J., Joffraud, M., and Giner, M. (2019). A reduced form of nicotinamide riboside defines a new path for NAD+ biosynthesis and acts as an orally bioavailable NAD+ precursor. Molecular metabolism *30*, 192-202.

Houtkooper, R.H., Pirinen, E., and Auwerx, J. (2012). Sirtuins as regulators of metabolism and healthspan. Nat Rev Mol Cell Bio *13*, 225-238.

Imai, S., Armstrong, C.M., Kaeberlein, M., and Guarente, L. (2000). Transcriptional

silencing and longevity protein Sir2 is an NAD-dependent histone deacetylase. Nature *403*, 795-800.

Imai, S., and Guarente, L. (2014). NAD(+) and sirtuins in aging and disease. Trends Cell Biol *24*, 464-471.

Katsyuba, E., Romani, M., Hofer, D., and Auwerx, J. (2020). NAD+ homeostasis in health and disease. Nature Metabolism *2*, 9-31.

Kosicki, G.W., and Lee, L.P. (1966). Effect of divalent metal ions on nucleotide inhibition of pig heart citrate synthase. J Biol Chem *241*, 3571-3574.

Kussmaul, L., and Hirst, J. (2006). The mechanism of superoxide production by NADH : ubiquinone oxidoreductase (complex I) from bovine heart mitochondria. P Natl Acad Sci USA *103*, 7607-7612.

Magni, G., Amici, A., Emanuelli, M., Orsomando, G., Raffaelli, N., and Ruggieri, S. (2004). Enzymology of NAD plus homeostasis in man. Cell Mol Life Sci *61*, 19-34.

Rajman, L., Chwalek, K., and Sinclair, D.A. (2018). Therapeutic Potential of NAD-Boosting Molecules: The In Vivo Evidence. Cell Metab *27*, 529-547.

Ryan, M.J., Johnson, G., Kirk, J., Fuerstenberg, S.M., Zager, R.A., and Torokstorb, B. (1994). Hk-2 - an Immortalized Proximal Tubule Epithelial-Cell Line from Normal Adult Human Kidney. Kidney Int *45*, 48-57.

Tang, H.P., Chen, Y.L., Liu, X.H., Wang, S.Y., Lv, Y., Wu, D., Wang, Q.T., Luo, M.K., and Deng, H.T. (2016). Downregulation of HSP60 disrupts mitochondrial proteostasis to promote tumorigenesis and progression in clear cell renal cell carcinoma. Oncotarget *7*, 38822-38834.

Teng, R.F., Liu, Z.Y., Tang, H.P., Zhang, W.H., Chen, Y.L., Xu, R.H., Chen, L., Song, J.P., Liu, X.H., and Deng, H.T. (2019). HSP60 silencing promotes Warburg-like phenotypes and switches the mitochondrial function from ATP production to biosynthesis in ccRCC cells. Redox Biol *24*.

Tilton, W.M., Seaman, C., Carriero, D., and Piomelli, S. (1991). Regulation of Glycolysis in the Erythrocyte - Role of the Lactate Pyruvate and Nad-Nadh Ratios. J Lab Clin Med *118*, 146-152.

Verbon, E.H., Post, J.A., and Boonstra, J. (2012). The influence of reactive oxygen species on cell cycle progression in mammalian cells. Gene *511*, 1-6.

Weiss, H., Friedrich, T., Hofhaus, G., and Preis, D. (1991). The respiratory-chain NADH dehydrogenase (complex I) of mitochondria. Eur J Biochem *197*, 563-576.

Wu, K.B., Knox, R., Sun, X.Z., Joseph, P., Jaiswal, A.K., Zhang, D., Deng, P.S.K., and Chen, S. (1997). Catalytic properties of NAD(P)H:quinone oxidoreductase-2 (NQO2), a dihydronicotinamide riboside dependent oxidoreductase. Arch Biochem Biophys *347*, 221-228.

Xiao, W.S., and Loscalzo, J. (2019). Metabolic Responses to Reductive Stress. Antioxid Redox Sign.

Yang, Y., Mohammed, F.S., Zhang, N., and Sauve, A.A. (2019). Dihydronicotinamide riboside is a potent NAD(+) concentration enhancer in vitro and in vivo. J Biol Chem *294*, 9295-9307.

Ying, W. (2008). NAD+/NADH and NADP+/NADPH in cellular functions and cell death: regulation and biological consequences. Antioxid Redox Signal *10*, 179-206.

Yoshino, J., Baur, J.A., and Imai, S.I. (2018). NAD(+) Intermediates: The Biology and Therapeutic Potential of NMN and NR. Cell Metab *27*, 513-528.

Yoshino, J., Mills, K.F., Yoon, M.J., and Imai, S.I. (2011). Nicotinamide Mononucleotide, a Key NAD(+) Intermediate, Treats the Pathophysiology of Diet- and Age-Induced Diabetes in Mice. Cell Metab *14*, 528-536.

Zhang, H.B., Ryu, D., Wu, Y.B., Gariani, K., Wang, X., Luan, P.L., D'Amico, D., Ropelle, E.R., Lutolf, M.P., Aebersold, R.*, et al.* (2016). NAD(+) repletion improves mitochondrial and stem cell function and enhances life span in mice. Science *352*, 1436-1443.

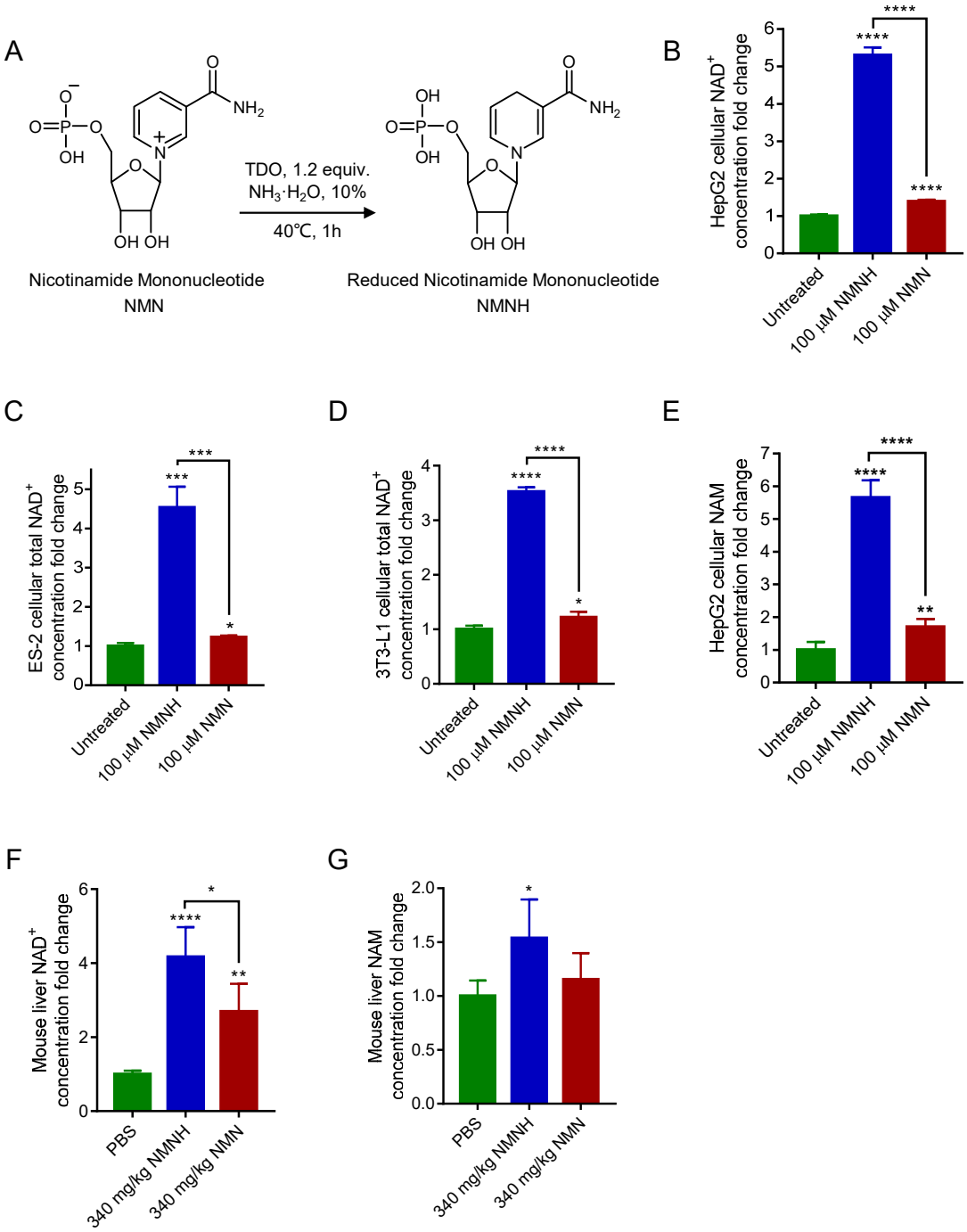

Figure 1. NMNH is potent NAD⁺ booster which is more effective than NMN

(A) NMNH synthesis procedure. NMNH was generated by reducing NMN with TDO under alkaline environment at 40 ℃ for 1 h.

(B) NMNH had better NAD⁺ enhancing effect than NMN in HepG2 cell. Cellular NAD⁺ concentration was determined after 100 μM NMN or NMNH treatment for 12 h using TSQ Quantiva mass spectrometer. Data are shown as mean ± SD (n = 4). ****p < 0.0001. Significance is obtained compared to the untreated group unless

otherwise specified.

(C) NMNH increased cellular total NAD^+ concentration in ES-2 cell. Cellular total NAD^+ concentration was determined after 100 μM NMN or NMNH treatment for 3 h using NAD^+ / NADH detecting kit (Beyotime, China). Data are shown as mean ± SD (n = 3). *p < 0.05, ***p < 0.001. Significance is obtained compared to the untreated group unless otherwise specified.

(D) NMNH increased cellular total NAD^+ concentration in 3T3-L1 cell. Cellular total NAD^+ concentration was determined after 100 μM NMN or NMNH treatment for 3 h using NAD^+ / NADH detecting kit (Beyotime, China). Data are shown as mean ± SD (n = 3). *p < 0.05, ****p < 0.0001. Significance is obtained compared to the untreated group unless otherwise specified.

(E) NMNH increased cellular NAM concentration in HepG2 cell. Cellular NAM concentration was determined after 100 μM NMN or NMNH treatment for 12 h using Q Exactive mass spectrometer. Data are shown as mean ± SD (n = 4). **p < 0.01, ****p < 0.0001. Significance is obtained compared to the untreated group unless otherwise specified.

(F) NMNH had better *in vivo* NAD^+ enhancing effect than NMN. C57BL/6J male mice were treated with 340 mg / kg NMN or NMNH for 6 h by intraperitoneal injection. Liver NAD^+ concentration was determined using TSQ Quantiva mass spectrometer. Data are shown as mean ± SD (n = 4). *p < 0.05, **p < 0.01, ****p < 0.0001. Significance is obtained compared to the untreated group unless otherwise specified.

(G) NMNH increased liver NAM concentration. C57BL/6J male mice were treated with 340 mg / kg NMN or NMNH for 6 h by intraperitoneal injection. Liver NAM concentration was determined using TSQ Quantiva mass spectrometer. Data are shown as mean ± SD (n = 4). *p < 0.05. Significance is obtained compared to the untreated group unless otherwise specified.

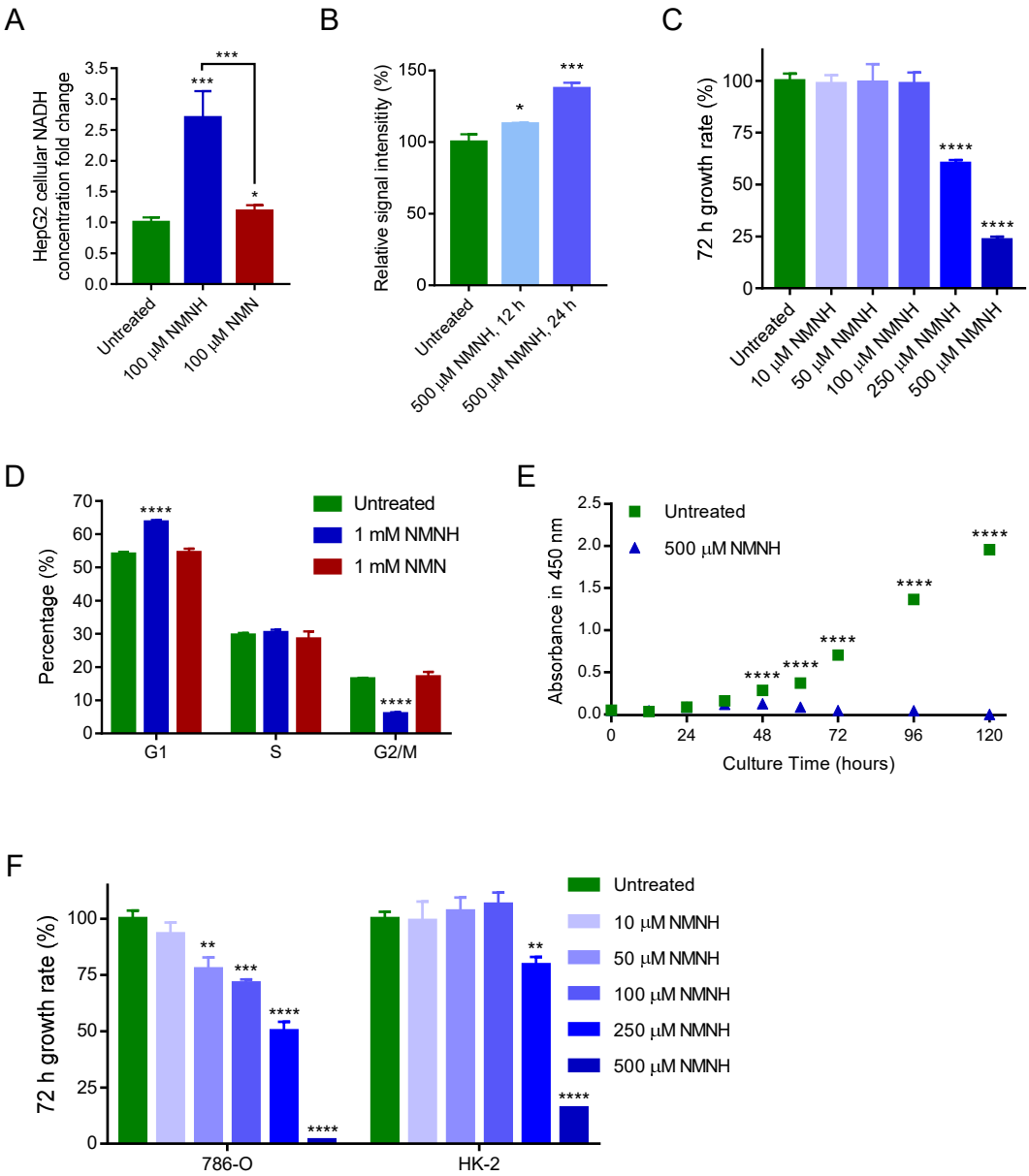

Figure 2. NMNH caused reductive stress and repressed cell growth

(A) NMNH increased cellular NADH concentration in HepG2 cell. Cellular NADH concentration was determined after 100 μM NMN or NMNH treatment for 12 h using TSQ Quantiva mass spectrometer. Data are shown as mean ± SD (n = 4). *p < 0.05, ***p < 0.001. Significance is obtained compared to the untreated group unless otherwise specified.

(B) NMNH increased cellular ROS level in HepG2 cell. Cellular ROS were determined after 500 μM NMNH treatment using CellROX® Deep Red Reagents (Invitrogen, NY). Data are shown as mean ± SD (n = 3). *p < 0.05, ***p < 0.001. Significance

is obtained compared to the untreated group unless otherwise specified.

(C) High concentration NMNH inhibited the growth of HepG2. Cell growth rates were determined after NMNH treatment for 72 h using CCK-8 (Dojindo, Kumamoto, Japan). Data are shown as mean ± SD (n = 3). **$p < 0.01$, ***$p < 0.001$. Significance is obtained compared to the untreated group unless otherwise specified.

(D) Percentages of G1phase, S phase, and G2/M phase subpopulations in differently treated HepG2 cells by cell cycle analysis. Data are shown as mean ± SD (n = 5). ****$p < 0.0001$. Significance is obtained compared to the untreated group unless otherwise specified.

(E) Growth curve of 786-O under 500 μM NMNH treatment. Cell growth rate were determined under 500 μM NMNH treatment using CCK-8 (Dojindo, Kumamoto, Japan). Data are shown as mean ± SD (n = 3). ****$p < 0.0001$. Significance is obtained compared to the untreated group unless otherwise specified.

(F) 786-O is more sensitive to NMNH compared to HK-2. Cell growth rates were determined after NMNH treatment for 72 h using CCK-8 (Dojindo, Kumamoto, Japan). Data are shown as mean ± SD (n = 3). **$p < 0.01$, ***$p < 0.001$. Significance is obtained compared to the untreated group unless otherwise specified.

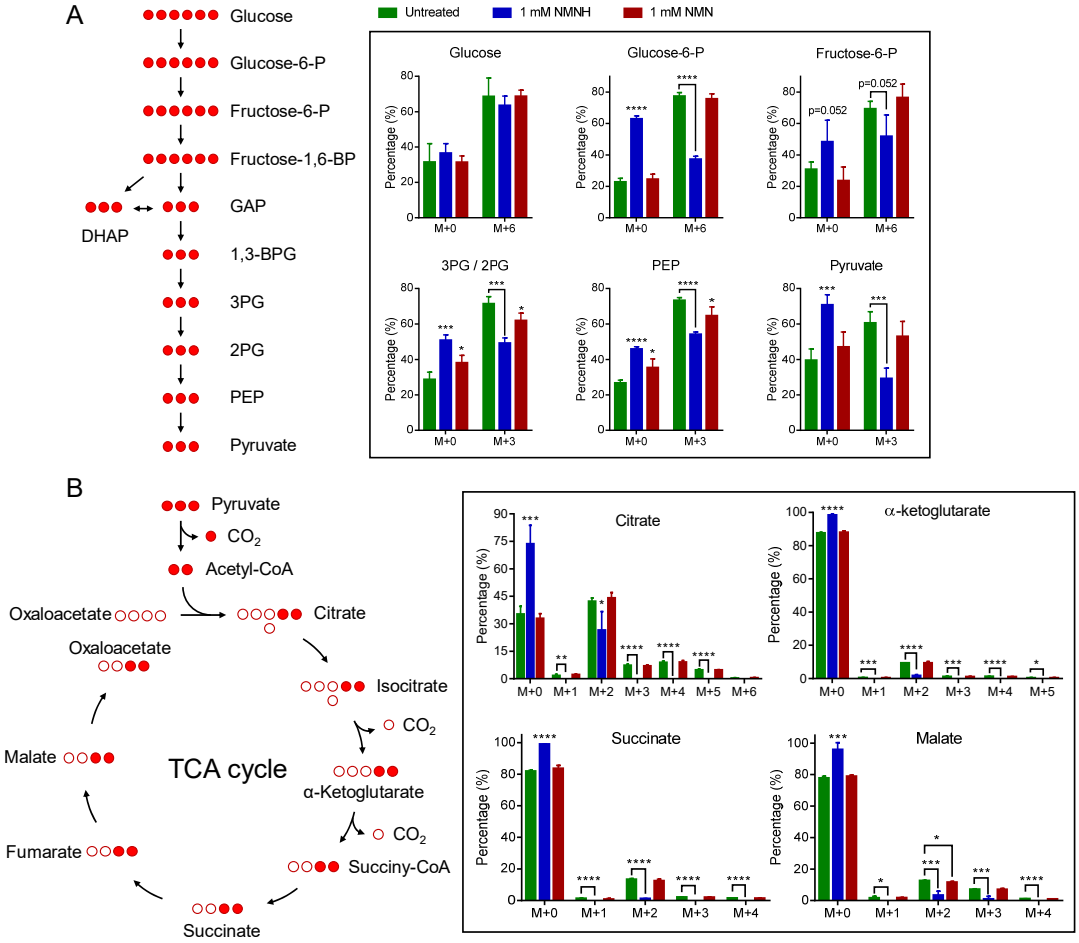

Figure 3. NMNH repressed glycolysis and TCA cycle

(A) Left, schematic of glycolysis. Red solid circle represents ^{13}C. Right, percentages of different isotope-encoded glycolysis metabolites. M+*n* represents a metabolite contains *n* ^{13}C atoms. Cellular metabolite concentrations were determined after 1 mM NMN or NMNH treatment in media supplied with U-$^{13}C_6$ glucose for 6 h using TSQ Quantiva mass spectrometer. Data are shown as mean ± SD (n = 4). *p < 0.05, ***p < 0.001, ****p < 0.0001. Glucose-6-P, glucose-6-phosphate. Fructose-6-P, fructose-6-phosphate. Fructose-1,6-BP, fructose-1,6-bisphosphate. GAP, glyceraldehyde-3-phosphate. DHAP, dihydroxyacetone phosphate. 1,3-BPG, 1,3-bisphosphoglycerate. 3PG / 2PG, 3-phosphoglycerate / 2-phosphoglycerate. PEP, phosphoenolpyruvate. Significance is obtained compared to the untreated group unless otherwise specified.

(B) Left, schematic of TCA cycle. Red solid circle represents ^{13}C. Right, percentages

of different isotope-encoded TCA cycle metabolites. M+*n* represents a metabolite contains *n* ^{13}C atoms. Cellular metabolite concentrations were determined after 1 mM NMN or NMNH treatment in media supplied with U-$^{13}C_6$ glucose for 6 h using TSQ Quantiva mass spectrometer. Data are shown as mean ± SD (n = 4). *$p < 0.05$, **$p < 0.01$, ***$p < 0.001$, ****$p < 0.0001$. Significance is obtained compared to the untreated group unless otherwise specified.

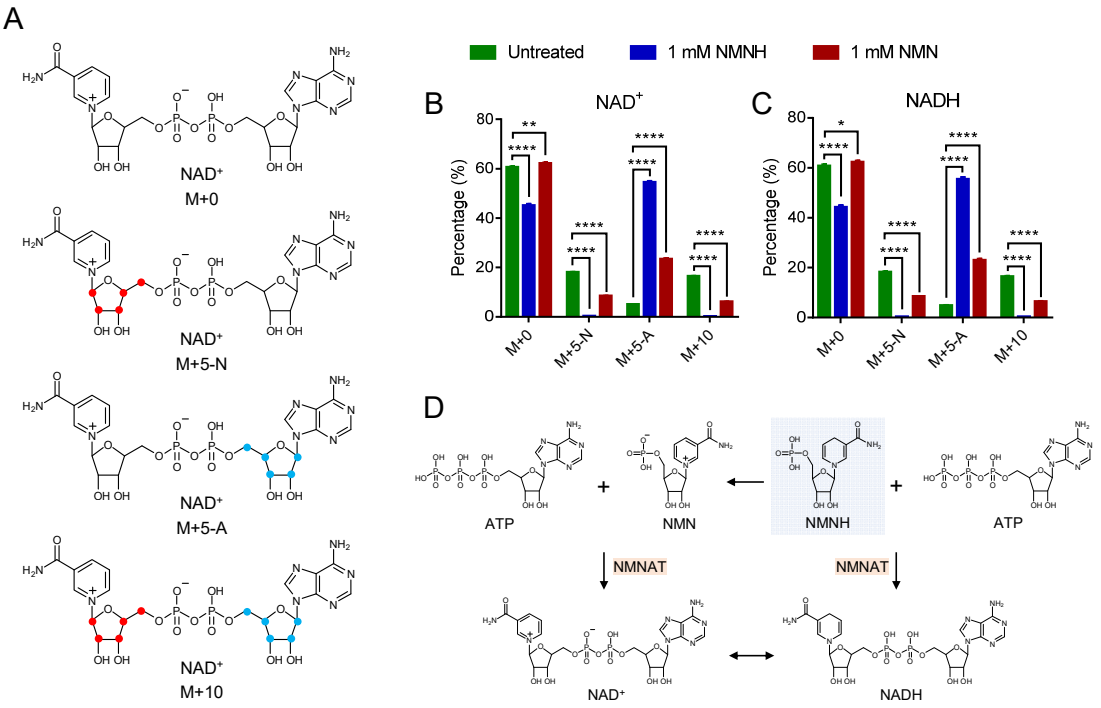

Figure 4. NMNH-induced NAD⁺ synthesis pathway Deconstructing

(A) NAD^+ label patterns. Red dots and blue dots represent ^{13}C atoms.

(B) Percentages of different isotope-encoded NAD^+. M+*n* represents NAD^+ contains *n* ^{13}C atoms. Cellular NAD^+ concentrations were determined after 1 mM NMN or NMNH treatment in media supplied with U-$^{13}C_6$ glucose for 6 h using TSQ Quantiva mass spectrometer. Data are shown as mean ± SD (n = 4). **$p < 0.01$, ****$p < 0.0001$. Significance is obtained compared to the untreated group unless otherwise specified.

(C) Percentages of different isotope-encoded NADH. M+*n* represents NADH contains *n* ^{13}C atoms. Cellular NADH concentrations were determined after 1 mM NMN or NMNH treatment in media supplied with U-$^{13}C_6$ glucose for 6 h using TSQ Quantiva mass spectrometer. Data are shown as mean ± SD (n = 4). *$p < 0.05$, ****$p < 0.0001$. Significance is obtained compared to the untreated group unless otherwise specified.

(D) Proposed metabolic pathway that NMNH was synthesized to NAD^+

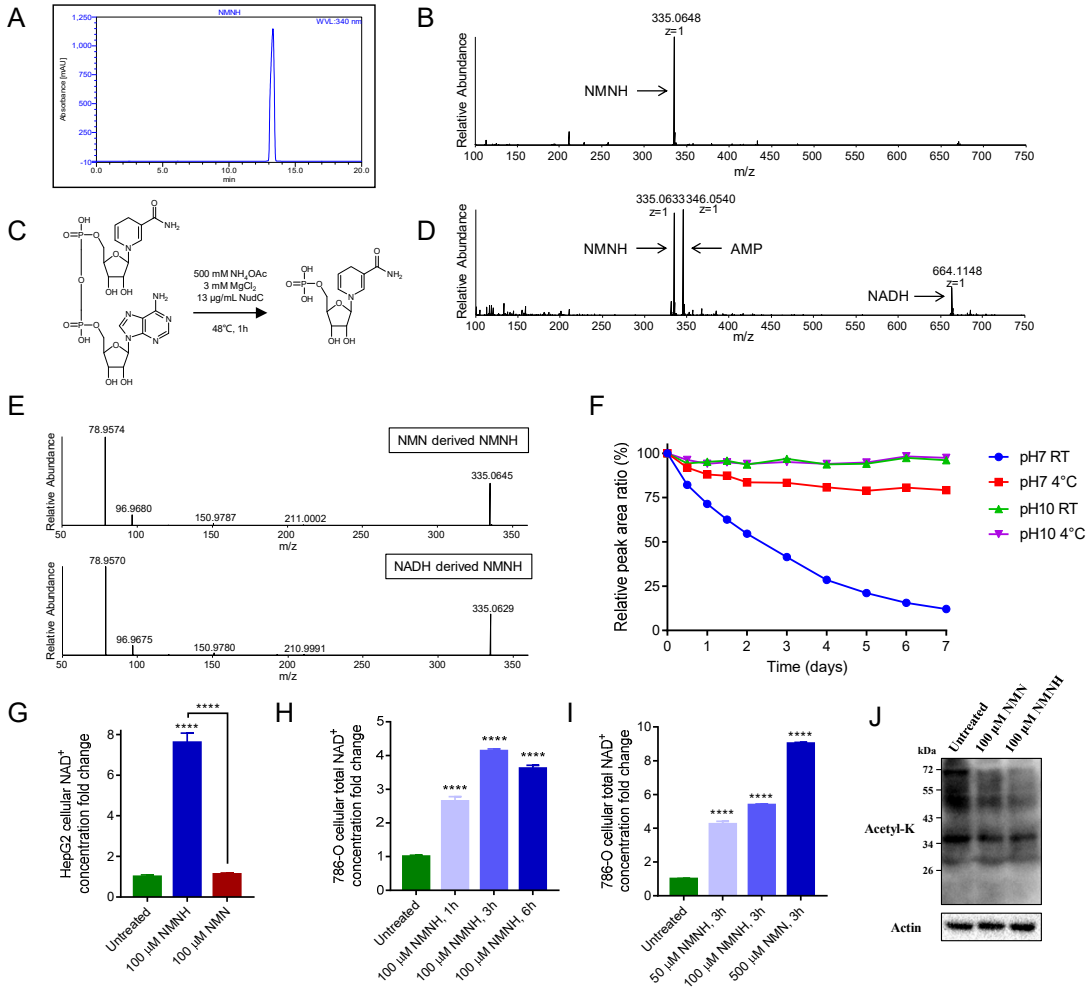

Figure S1. Molecular features and verification of NMNH

(A) Characteristic UV absorption peak of NMNH. NMNH has a UV absorption centered at 340 nm.

(B) MS spectrum feature of NMNH generated by NMN reduction. NMNH has an m/z of 335.0648 in negative ion mode.

(C) Procedure of NMNH generation by NADH decomposition. NMNH was generated by decomposing NADH using NudC

(D) MS spectrum feature of NMNH generated by NADH decomposition. NMNH has an m/z of 335.0633 in negative ion mode.

(E) MS/MS spectra comparison of enzymatically- and chemically-generated NMNH. NMNH generated by NMN reduction has the identical fragmentation pattern as NMNH generated by NADH decomposition.

(F) NMNH is stable under alkaline and low-temperature environment. Equal amount

of NMNH were stored under different conditions and their 340 nm absorptions were determined.

(G) NMNH had better NAD^+ enhancing effect than NMN in HepG2 cell. Cellular NAD^+ concentration was determined after 100 μM NMN or NMNH treatment for 12 h using Q Exactive mass spectrometer. Data are shown as mean ± SD (n = 4). ****$p < 0.0001$. Significance is obtained compared to the untreated group unless otherwise specified.

(H) NMNH increased cellular total NAD^+ concentration in 786-O cell. Cellular total NAD^+ concentration was determined after 100 μM NMN or NMNH treatment for 1-6 h using NAD^+ / NADH detecting kit (Beyotime, China). Data are shown as mean ± SD (n = 3). ****$p < 0.0001$. Significance is obtained compared to the untreated group unless otherwise specified.

(I) NMNH increased cellular total NAD^+ concentration in 786-O cell. Cellular total NAD^+ concentration was determined after 50-500 μM NMN or NMNH treatment for 3 h using NAD^+ / NADH detecting kit (Beyotime, China). Data are shown as mean ± SD (n = 3). ****$p < 0.0001$. Significance is obtained compared to the untreated group unless otherwise specified.

(J) NMNH promoted cellular deacetylation activity. HepG2 cells were treated with 100 μM NMN or NMNH for 24 h and proteins were extracted for western blot analysis following standard protocol.

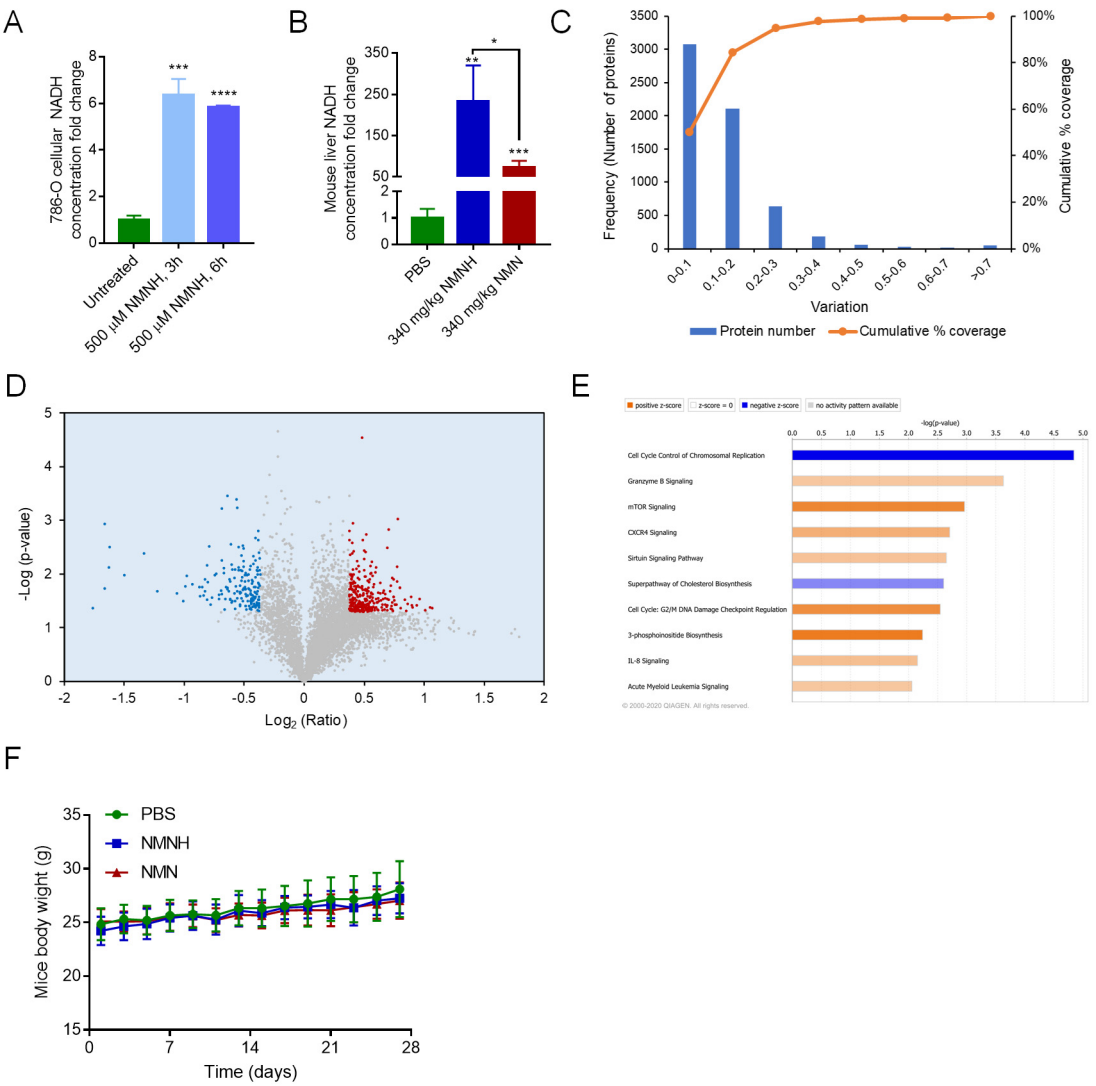

Figure S2. NMNH increased cellular NADH level and repressed cell growth

(A) Cellular NADH concentration was determined after 500 μM NMN or NMNH treatment using NAD^+ / NADH detecting kit (Beyotime, China). Data are shown as mean ± SD (n = 3). ***p < 0.001, ****p < 0.0001. Significance is obtained compared to the untreated group unless otherwise specified.

(B) NMNH increased liver NADH concentration. C57BL/6J male mice were treated with 340 mg / kg NMN or NMNH for 6 h by intraperitoneal injection. Liver NADH concentration was determined using TSQ Quantiva mass spectrometer. Data are shown as mean ± SD (n = 4). *p < 0.05, **p < 0.01. Significance is obtained compared to the untreated group unless otherwise specified.

(C) Determination of experimental variation and cutoff value for the identified proteins.

Horizontal axis represents TMT ratio variation. Primary vertical axis represents the number of proteins with corresponding different variation. Secondary vertical axis represents the cumulative percentage coverage of the counted proteins. Cutoff value was set according to the variation against 88% coverage of population.

(D) Volcano plot obtained from TMT-based quantitative proteomics analysis. Red dots represent proteins exhibiting significative un-regulated fold changes. Blue dots represent proteins exhibiting significative down-regulated fold changes.

(E) Representative canonical pathways enriched IPA (Ingenuity Pathway Analysis) software.

(F) Mice body weight curves under NMNH or NMN treatment. C57BL/6J male mice were treated with 13.6 mg / kg NMN or NMNH every day for 4 weeks by intraperitoneal injection. Data are shown as mean ± SD (n = 5).

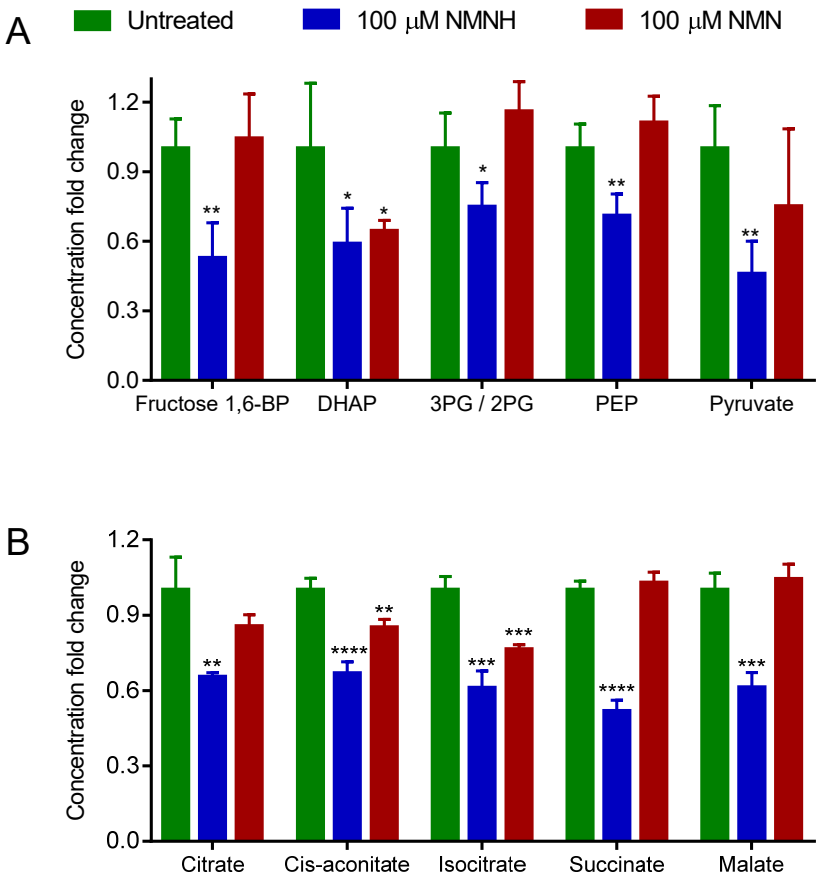

Figure S3. Metabolomic analysis of TCA intermediates under NMNH and NMN treatment.

(A) NMNH decreased glycolysis intermediate concentrations in HepG2 cell. Cellular metabolite concentrations were determined after 100 μM NMN or NMNH treatment for 12 h using TSQ Quantiva mass spectrometer. Data are shown as mean ± SD (n = 4). *p < 0.05, **p < 0.01. Fructose-1,6-BP, fructose-1,6-bisphosphate. DHAP, dihydroxyacetone phosphate. 3PG / 2PG, 3-phosphoglycerate / 2-phosphoglycerate. PEP, phosphoenolpyruvate. Significance is obtained compared to the untreated group unless otherwise specified.

(B) NMNH decreased TCA cycle intermediate concentrations in HepG2 cell. Cellular metabolite concentrations were determined after 100 μM NMN or NMNH treatment for 12 h using TSQ Quantiva mass spectrometer. Data are shown as mean ± SD (n = 4). **p < 0.01, ***p < 0.001, ****p < 0.0001. Significance is obtained compared to the untreated group unless otherwise specified.

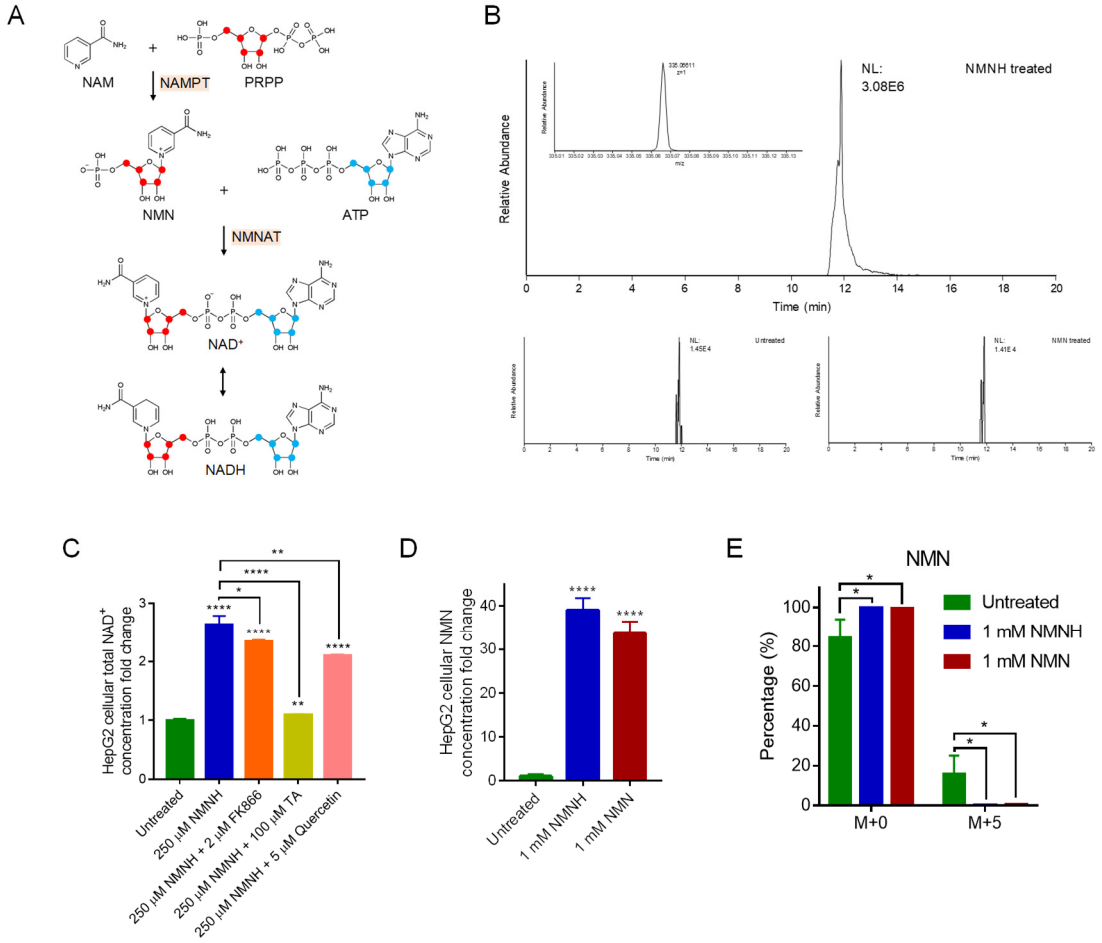

Figure S4. NMNH-induced NAD⁺ synthesis pathway Deconstructing

(A) Schematic representation of the salvage pathway. Red dots and blue dots represent ^{13}C atoms.

(B) MS spectrum of NMNH. The embedded figure represents the mass of NMNH in negative ion mode detected by Q Exactive mass spectrometer. NL represents signal intensity.

(C) NMNH increased cellular NAD^+ levels depending on NMNAT. Cells were treated by different kinds of inhibitors for 1 hour before NMNH treatment. Cellular total NAD^+ concentration was determined after 250 μM NMNH treatment for 1 h using NAD^+ / NADH detecting kit (Beyotime, China). Data are shown as mean ± SD (n = 3). *p < 0.05, **p < 0.01, ****p < 0.0001. Significance is obtained compared to the untreated group unless otherwise specified.

(D) NMNH increased cellular NMN concentration in HepG2 cell. Cellular NMN

concentration was determined after 1 mM NMN or NMNH treatment for 6 h using Q Exactive mass spectrometer. Data are shown as mean ± SD (n = 4). ****$p < 0.0001$.

(E) Percentages of different isotope-encoded NMN. M+*n* represents NMN contains *n* ^{13}C atoms. Cellular NMN concentrations were determined after 1 mM NMN or NMNH treatment in media supplied with U-$^{13}C_6$ glucose for 6 h using Q Exactive mass spectrometer. Data are shown as mean ± SD (n = 4).